Cite this: *Gen. Chem.* **2017**, *3*, 172. DOI: 10.21127/yaoyigc20170017

Tailoring Iron Oxide Nanostructures for High-Capacity Lithium Storage

Yao Yao, Jiantao Li, Qinyou An, Liqiang Mai,* and Liang Zhou*

State Key Laboratory of Advanced Technology for Materials Synthesis and Processing, International School of Materials Science and Engineering, Wuhan University of Technology, Wuhan, Hubei 430070, China

Iron oxides, such as hematite (α-Fe_2O_3), maghemite (γ-Fe_2O_3), and magnetite (Fe_3O_4), have been considered as alternative anode materials for lithium-ion batteries (LIBs) due to their high theoretical capacity, abundant reserves, low cost, and non-toxicity. However, their practical application has been hampered by the large volume expansion, which leads to rapid capacity fading. Nanostructure engineering has been demonstrated to be an effective avenue in tackling the volume variation issue and boosting the electrochemical performances. Herein, recent advances on nanostructure engineering of iron oxides for lithium storage are summarized. These nanostructures include 0D nanoparticles, 1D nanowires/nanorods/nanofibers/nanotubes, 2D nanoflakes/nanosheets, as well as 3D porous/hollow/hierarchical architectures. The structure-electrochemical performance correlations are also discussed. It is believed that the performance optimization strategies summarized here might be extended to other high-capacity LIB anode materials.

Keywords iron oxide, nanostructure, nanocomposite, lithium storage, anode

Introduction

The global concerns of energy shortage and environmental pollution make the clean and sustainable energy an urgent need.[1-3] With high energy density and long lifespan, rechargeable lithium-ion batteries (LIBs) are one of the most promising energy storage devices for portable electronics and electric vehicles. However, the current state-of-the-art LIBs can't meet the ever increasing demands on energy density. The current commercialized graphite-based anode suffers from low specific capacity (372 $mAh \cdot g^{-1}$) and poor safety. Therefore, exploring alternative anode materials with high capacity and good safety has attracted growing attention.[4-16]

Transition metal oxides (TMOs) represent a promising family of high-capacity anode materials for LIBs.[17] Based on a conversion reaction mechanism, they are able to provide a specific capacity of 700–1000 $mAh \cdot g^{-1}$, which is two to three times to that of graphite. Among the various TMOs, iron oxides, such as hematite (α-Fe_2O_3), maghemite (γ-Fe_2O_3), and magnetite (Fe_3O_4), have attracted particular attention due to their high theoretical capacity, abundant reserves, low cost, and non-toxicity.[18,19] Take the Fe_2O_3 as an example, each formular of Fe_2O_3 is able to react with 6 Li^+, providing a high theoretical capacity of 1007 $mAh \cdot g^{-1}$. However, the high specific capacity is accompanied by a large volume change (~96%) during lithiation/de-lithiation.[20] Such a large volume variation results in the notorious problems of active material pulverization, electrode disintegration (loss of electrical contact between active material and current collector), and unstable solid electrolyte interphase (SEI) film formation, eventually leading to rapid capacity fading upon cycling. To achieve high specific capacity without compromising the cyclability, the volume change associated with repeated lithiation/de-lithiation should be better accommodated.

Nanostructure engineering has been demonstrated to be an effective avenue in tackling the volume expansion issue of high-capacity anode materials. The strain induced by lithiation/de-lithiation can be effectively alleviated by proper nanostructure design. Especially, if sufficient pores/voids were introduced in the active material, the volume change of electrode materials can be accommodated as well. Other benefits of nanostructured electrode materials include reduced Li^+ diffusion lengths and high electrode/electrolyte contact area for Li^+ flux.[21-23] This review provides a comprehensive summarization of the recent advances on nanostructure engineering of iron oxides for lithium storage. These nanostructures include 0-dimensional (0D) nanoparticles, 1D nanowires/nanorods/nanofibers/nanotubes, 2D nanoflakes/nanosheets, and 3D porous/hollow/hierarchical structures. The structure-electrochemical performance correlations are also discussed.

α-Fe_2O_3 based anode materials

Hematite, also known as α-Fe_2O_3, is the most thermodynamically stable form of iron oxide under ambient conditions.[24] It has a corundum structure, in which oxygen adopts a hexagonal close packing while Fe occupies two-thirds of the octahedral vacancy sites. Despite its high theoretical capacity, α-Fe_2O_3 suffers from large volume expansion (~96%) during lithiation and low intrinsic conductivity. To tackle these issues, it is necessary to design α-Fe_2O_3 nanostructures with improved structural stability and electronic conductivity.

α-Fe_2O_3 based 1D nanostructures

1D nanowires, nanorods, nanofibers, and nanotubes possess multiple merits in lithium storage, including large electrode-electrolyte contact area, facile strain relaxation, and efficient 1D electron transport pathways.[25] In 2006, Xie *et al.* reported the first discharge/charge profiles of α-Fe_2O_3 nanorods.[26] Later, Tang's group reported the initial discharge/charge curves of α-Fe_2O_3.[27] Although the long-term cycling performances were not provided, these studies suggest that α-Fe_2O_3 nanorods could be used as high-capacity LIB anode. Wang *et al.* studied the electrochemical performances of single crystalline α-Fe_2O_3 nanorods with diameters of 60–80 nm.[28] The

* E-mail: liangzhou@whut.edu.cn, mlq518@whut.edu.cn
Received September 28, 2017; accepted November 20, 2017.

α-Fe_2O_3 nanorods demonstrated a high reversible capacity of 955 mAh·g^{-1}; the capacity decreased to 763 mA·h·g^{-1} after 30 cycles. Recently, Mullins *et al.* studied the lithium storage performances of hydrothermally synthesized single-crystalline α-Fe_2O_3 nanorods with average diameters of ~40 nm and lengths of ~400 nm.[20] The sample exhibited a stable capacity of ~ 930 mAh·g^{-1} from the 2nd to the 30th cycle.

Introducing porosity in α-Fe_2O_3 1D nanostructures can further boost their electrochemical performances due to their volume change accommodation and strain relaxation abilities.[29-33] Liu *et al.* prepared porous single-crystalline α-Fe_2O_3 nanorod array on Ti foil by a hydrothermal method followed by annealing.[30] The α-Fe_2O_3 nanorod array could be directly used as additive-free LIB anode, delivering a capacity of 562 mAh·g^{-1} after 50 cycles. Liu, Xu, and co-workers synthesized α-Fe_2O_3 porous nanorods with diameters of 30–60 nm (Figure 1a) through thermal decomposition of $FeC_2O_4·2H_2O$ nanorods.[31] The α-Fe_2O_3 porous nanorods delivered a high discharge capacity of 916 mAh·g^{-1} after 100 cycles at 1C (1C=1000–1007 mA·g^{-1}). Recently, Mai and co-workers fabricated a series of α-Fe_2O_3 1D nanostructures, including hierarchical nanotubes, porous nanotubes, and ladder-like nanostructures (Figures 1b, 1c), by a template-engaged redox reaction followed by thermal treatment.[33] The α-Fe_2O_3 ladder-like nanostructure delivered a stable capacity of over 1100 mAh·g^{-1} at 0.1 C. Even at a high rate of 5C, the sample exhibited a capacity of 645 mAh·g^{-1} after 1200 cycles.

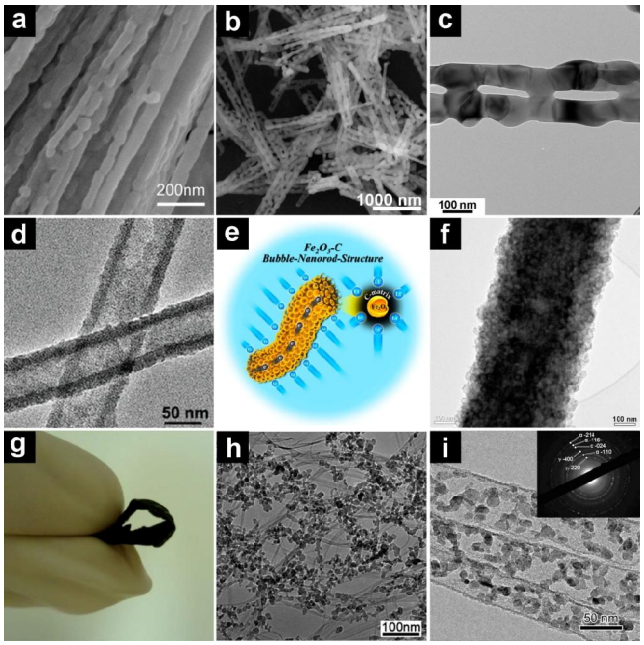

Figure 1 SEM image of α-Fe_2O_3 porous nanorods (a);[31] SEM (b) and TEM (c) images of α-Fe_2O_3 ladder-like nanostructure;[33] TEM images of α-Fe_2O_3 nanotubes (d);[35] schematic illustration (e) and TEM image (f) of α-Fe_2O_3-carbon composite nanofibers constructed by α-Fe_2O_3 nanobubbles dispersed in an amorphous carbon matrix;[41] digital photo of a flexible α-Fe_2O_3-SWCNT membrane (g), TEM image of α-Fe_2O_3-SWCNT (h), TEM image of Fe_2O_3 nanoparticle filled CNT (i).[44]

Nanotubes with efficient Li^+ diffusion channels and sufficient free space for volume expansion have also been demonstrated to be a promising electrode structure.[34-37] In 2005, Chen's group studied the lithium storage performances of α-Fe_2O_3 nanotubes prepared by hard templating.[34] The α-Fe_2O_3 nanotubes delivered an initial discharge capacity of 1415 mAh·g^{-1}; the capacity decreased to 510 mAh·g^{-1} after 100 cycles. Using ZnO nanowire array as the template, Liu and co-workers synthesized vertically aligned α-Fe_2O_3 nanotubes on alloy substrate through a "sacrificial template-accelerated hydrolysis" approach.[36] This synthetic strategy could be extended to the preparation of α-Fe_2O_3-SnO_2 nanotube array on stainless steel substrate.[38] The obtained nanotube arrays could function as additive-free LIB anode materials. Using Cu nanowires as the sacrificial templates, Lou *et al.* prepared α-Fe_2O_3 nanotubes with diameters of 50–200 (Figure 1d).[35] The as-obtained α-Fe_2O_3 nanotubes exhibited a high specific capacity of over 1000 mAh·g^{-1} at 0.5 C with excellent cycling stability. Chaudhari and Srinivasan synthesized α-Fe_2O_3 hollow nanofibers by electrospinning, which showed a high reversible capacity of 1293 mAh·g^{-1} at 0.06 C with good cycling stability.[37]

Compositing the 1D α-Fe_2O_3 nanostructures with conductive carbon would integrate the advantages of both materials, further boosting the lithium storage performance.[39-42] For example, α-Fe_2O_3-carbon nanofibers (α-Fe_2O_3-CNF) were prepared via electrospinning and evaluated as LIB anode materials by different groups.[39-41] The α-Fe_2O_3-carbon composite nanofibers prepared by Fan *et al.* demonstrated a stable capacity of ~820 mAh·g^{-1} at 0.2 C for 100 cycles.[40] The α-Fe_2O_3-carbon composite nanofibers prepared by Kang's group were constructed by numerous α-Fe_2O_3 nanobubbles uniformly dispersed in an amorphous carbon matrix (Figures 1e and 1f).[41] This novel nanostructure delivered a high specific capacity of ~820 mAh·g^{-1} after 300 cycles at 1 C.

Fe_2O_3-carbon nanotube (Fe_2O_3-CNT) composites have also been constructed and evaluated as LIB anode materials.[43-45] The Fe_2O_3 nanoparticles can be either decorated on or confined in the CNTs. For example, Li *et al.* designed an α-Fe_2O_3 nanoparticle decorated single-walled carbon nanotube (α-Fe_2O_3-SWCNT) membrane with a high Fe_2O_3 loading of 88 wt% (Figures 1g and 1h).[43] The α-Fe_2O_3-SWCNT membrane can function as a flexible, binder-free, and current-collector-free LIB anode, demonstrating a high reversible capacity of 1243 mAh·g^{-1} at 0.05 C and a specific capacity of 801 mAh·g^{-1} after 90 cycles as 0.5 C. Liu *et al.* constructed an Fe_2O_3 nanoparticle filled CNT composite (Fe_2O_3-CNT) with α-Fe_2O_3 as the major phase and γ-Fe_2O_3 as the minor phase (Figure 1i).[44] A capacity of 811 mAh·g^{-1} could be achieved after 100 cycles at 0.035 C. The superior electrochemical properties of the Fe_2O_3-CNT could be attributed to its unique configuration, where the CNT shell not only improved the electronic conductivity but also prevented the aggregation and exfoliation of the Fe_2O_3 nanoparticles during repeated discharge/charge processes.

α-Fe_2O_3 based 2D nanostructures

2D nanoflakes/nanosheets/nanodiscs are able to expand/contract in the direction parallel to the normal of the basal plane during lithiation/de-lithiation.[46-48] In 2006, Chowdari *et al.* reported the preparation of α-Fe_2O_3 nanoflakes (Figure 2a) on Cu foil via a thermal treatment method.[46] The α-Fe_2O_3 nanoflakes exhibited a stable capacity of ~700 mAh·g^{-1} at 0.065 C with no noticeable capacity fading for 80 cycles. Using a solvothermal method with subsequent annealing, Lou *et al.* grew porous α-Fe_2O_3 nanosheets (Figure 2b) on various metallic substrates.[47] With highly porous and ultrathin features, the Ti foil supported α-Fe_2O_3 nanosheets provided a specific capacity of 908 mAh·g^{-1} after 60 cycles at 0.1 C.

Graphene, a typical 2D material with excellent electronic conductivity, high surface area, mechanical robustness, is an ideal component to couple with α-Fe_2O_3 for volume change accommodation and conductivity improvement.[49-60] Therefore, α-Fe_2O_3-graphene nanocomposites have been extensively investigated for lithium storage. As a typical example, Ruoff's group prepared an α-Fe_2O_3-reduced graphene oxide composite (α-Fe_2O_3-RGO), which manifested a reversible capacity of 982 mAh·g^{-1} with good capacity retention.[49] Li *et al.* constructed a monolithic α-Fe_2O_3-graphene hybrid (Figures 2c and 2d) by a hydrothermal approach.[59] The resultant hybrid could be directly used as a free-standing LIB anode, providing a specific

capacity of 810 mAh·g^{-1} after 100 cycles at 0.1 C. In another study, Wang *et al*. designed an α-Fe_2O_3-CNT-graphene ternary hybrid (Figure 2e) by a chemical vapor deposition (CVD) method.[57] When applied as the anode material for LIBs, the ternary hybrid manifested high specific capacity (984 mAh·g^{-1}), superior cyclability, and high rate capability.

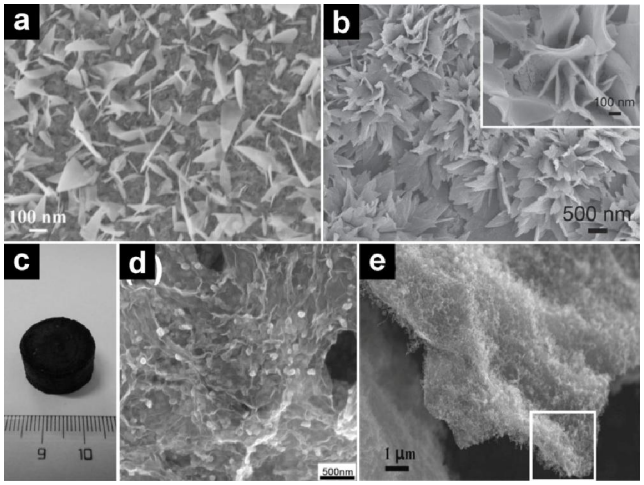

Figure 2 SEM image of α-Fe_2O_3 nanoflakes on Cu foil (a),[46] SEM image of α-Fe_2O_3 nanosheets on Ti foil (b),[47] digital photo of the monolithic α-Fe_2O_3-graphene hybrid (c); SEM image of the α-Fe_2O_3-graphene hybrid (d),[59] SEM image of the α-Fe_2O_3-CNT-graphene ternary composite (e).[57]

α-Fe_2O_3 based 3D nanostructures

3D porous/hollow/hierarchical structures are able to integrate the advantages of both nanosized primary particles and micron-sized secondary assemblies.[61] Among the various 3D architectures, hollow structures attracted the most attention due to their unique merits of hollow cavity for volume change accommodation, reduced lengths for Li^+ diffusion, and abundant lithium storage sites.[62-66] In 2007, the lithium storage properties of α-Fe_2O_3 hollow spindles and microspheres were reported by Tang and co-workers.[67] Later, Xie's group reported the anode performance of α-Fe_2O_3 hollow spheres with a mesoporous shell.[68] In 2009, Song *et al.* reported a Kirkendall-effect-assisted strategy for the fabrication of α-Fe_2O_3 (Figures 3a and 3b) and carbon encapsulated α-Fe_2O_3 (α-Fe_2O_3@C) hollow nanoparticles.[69] The synthesis generally involved two steps, the preparation of Fe_3C@C nanoparticles via co-carbonization and the controlled oxidation of Fe_3C@C nanoparticles. During the controlled oxidation, Fe_3C@C was converted into either α-Fe_2O_3@C (280 °C for 5 h) or pure α-Fe_2O_3 hollow nanoparticles (280 °C for 24 h) through nanoscale Kirkendall effect. The outer semi-graphitic carbon shell could solve the volume expansion and aggregation issues of α-Fe_2O_3 effectively. As a result, the α-Fe_2O_3@C hollow nanoparticles demonstrated significantly improved cyclability when compared to the pristine α-Fe_2O_3 hollow nanoparticles.

Hierarchical hollow spheres constructed by nanosheets/nanoneedles were fabricated and evaluated in LIBs by several groups.[70-73] Lou's group developed a quasi-emulsion tempating method for the synthesis of α-Fe_2O_3 hollow spheres with sheet-like building blocks, which delivered a capacity of 710 mAh·g^{-1} after 100 cycles at 0.2 C.[70] The same group also performed a comparative study on the lithium storage performances of hollow and solid α-Fe_2O_3 urchin-like spheres (Figures 3c and 3d).[71] It was found that the hollow α-Fe_2O_3 urchin-like spheres manifested better electrochemical performances than the solid counterpart in terms of specific capacity and capacity retention. Zhang, Yan, and co-workers prepared α-Fe_2O_3 hierarchical hollow spheres constructed by ultrathin nanosheets (Figures 3e and 3f) via a sacrificial templating process.[72] The product provided a reversible capacity of 920 mAh·g^{-1}, retaining 815 mAh·g^{-1} after 200 cycles. The superior electrochemical performances were ascribed to the synergistic effect of the hollow structure and ultrathin nanosheets. To further boost the electrochemical performances of α-Fe_2O_3 hierarchical hollow spheres, Huh and co-workers fabricated α-Fe_2O_3@polyaniline (α-Fe_2O_3@PANI) core@shell hierarchical hollow spheres (Figures 3g and 3h) through a simultaneous etching and polymerization process.[73] As expected, the α-Fe_2O_3@PANI core@shell yielded significantly enhanced electrochemical performances in terms of cyclability and rate capability, when compared to pristine urchin-like α-Fe_2O_3 hierarchical hollow spheres.

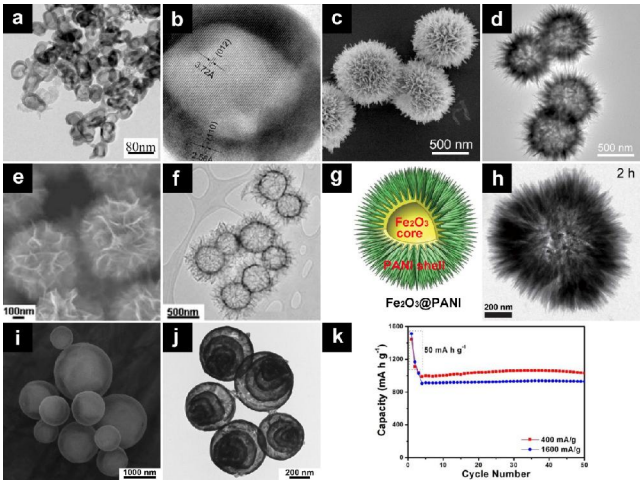

Figure 3 TEM images of α-Fe_2O_3 hollow nanoparticles (a, b);[69] SEM (c) and TEM (d) images of hollow α-Fe_2O_3 urchin-like spheres;[71] SEM (e) and TEM (f) images of α-Fe_2O_3 hierarchical hollow spheres constructed by ultrathin nanosheets;[72] schematic illustration (g) and TEM image (h) of α-Fe_2O_3@PANI core@shell hierarchical hollow spheres;[73] SEM (i), TEM (j) images and cycling performances of α-Fe_2O_3 multi-shelled hollow spheres.[74]

Despite the multiple merits, hollow structures usually suffer from low tap density, which would sacrifice the volumetric energy density when applied in LIBs. In this regard, multi-shelled hollow structures are advantageous over the single-shelled counterparts. Recently, Zhou *et al.* developed a simple spray drying method for the preparation of α-Fe_2O_3 multi-shelled hollow spheres using cheap, widely available iron nitrate and sucrose as the only precursors.[74,75] The obtained α-Fe_2O_3 presented a unique quadruple-shelled hollow spherical structure with sizes of 300–3000 nm (Figures 3i and 3j). The non-equilibrium heat treatment induced heterogeneous contraction was responsible for the formation of the multi-shelled hollow structures. When evaluated as the LIB anode material, the α-Fe_2O_3 MSHSs delivered stable high capacities of 1000 and 900 mAh·g^{-1} with no noticeable capacity fading up to 50 cycles at 0.4 and 1.6 C, respectively (Figure 3k). Similar α-Fe_2O_3 multi-shelled hollow structures could be achieved by hard templating[76] and spray pyrolysis.[77]

Other α-Fe_2O_3-based 3D architectures employed in LIBs include mesoporous α-Fe_2O_3,[78-80] porous α-Fe_2O_3,[61,81] α-Fe_2O_3@graphitic carbon microspheres,[82] α-Fe_2O_3@C hierarchical tubular structures (a),[83] α-Fe_2O_3@C hollow nanohorns on CNT (Figure 4b),[84] hierarchical SnO_2-Fe_2O_3 heterostructures,[85] hierarchical TiO_2@α-Fe_2O_3 hollow structures (Figure 4c),[86] branched TiO_2-B@α-Fe_2O_3 heterostructures (Figure 4d),[87] branched SnO_2@α-Fe_2O_3 heterostructures (Figure 4e),[88] and branched β-MnO_2@α-Fe_2O_3 heterostructures (Figure 4f).[89] All these 3D architectures demonstrated impressive lithium storage performances.

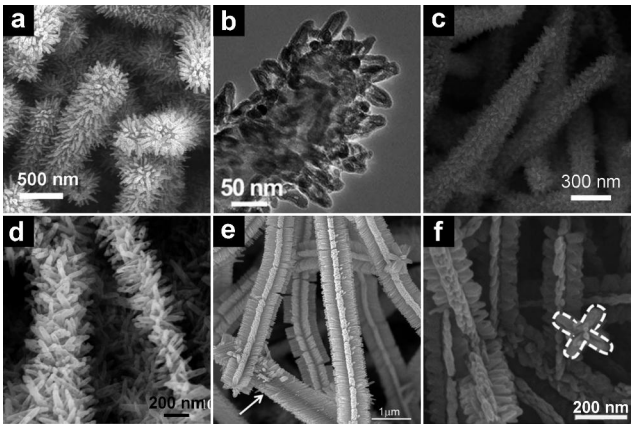

Figure 4 SEM image of α-Fe_2O_3@C hierarchical tubular structures (a),[83] TEM image of α-Fe_2O_3@C hollow nanohorns on CNT (b),[84] SEM image of TiO_2@α-Fe_2O_3 hollow structures (c),[86] SEM image of branched TiO_2-B@α-Fe_2O_3 heterostructures (d),[87] SEM image of branched SnO_2@α-Fe_2O_3 heterostructures (e),[88] SEM image of branched β-MnO_2@α-Fe_2O_3 heterostructures (f).[89]

γ-Fe_2O_3 based anode materials

γ-Fe_2O_3 adopts a cubic crystal structure with $FD\bar{3}m$ space group. In the unit cell, the Fe^{3+} ions occupy the octahedral 16d and tetrahedral 8a sites with different chemical states. Compared to the numerous publications on α-Fe_2O_3 based anode materials, the reports on γ-Fe_2O_3 based anode materials are much less, probably due to its poor stability.

Gamma-Fe_2O_3 based 1D nanostructures

The 1D γ-Fe_2O_3 based anode materials include Fe_2O_3 nanotubes,[90] Fe_2O_3-CNT hybrids,[42,91] and γ-Fe_2O_3-carbon nanofiber.[92-94] Son reported the synthesis of 1D Fe_2O_3 nanotubes (γ-Fe_2O_3 as the dominant phase and α-Fe_2O_3 as the minor phase) with particulate walls using microporous organic tubes as the templates.[90] The resultant Fe_2O_3 nanotubes delivered a discharge capacity of 950 mAh·g^{-1} for the second cycle, maintaining 929 mAh·g^{-1} after 30 cycles. Liu *et al*. designed an Fe_2O_3-CNT nanocomposite (γ-Fe_2O_3 as the dominant phase and α-Fe_2O_3 as the minor phase) with 9 nm-Fe_2O_3 nanoparticles homogeneously filled in the hollow interiors of CNTs.[42] The Fe_2O_3-NT nanocomposite showed a specific capacity of 768 mAh·g^{-1} after 40 cycles. Cheng and co-workers fabricated two types of γ-Fe_2O_3-CNT hybrids, γ-Fe_2O_3 nanoparticle-filled CNT (Figure 5a) and γ-Fe_2O_3 nanoparticle-coated CNT (Figure 5b).[91] The γ-Fe_2O_3 nanoparticle-coated CNT with an Fe_2O_3 mass ratio of 45 % exhibited a reversible capacity of 1092 mAh·g^{-1} at 50 mA·g^{-1}; the capacity decreased to 867 mAh·g^{-1} after 16 cycles. Meanwhile, the γ-Fe_2O_3 nanoparticle-filled CNT with a Fe_2O_3 weight ratio of 20 % delivered a reversible capacity of 1144 mAh·g^{-1}; the capacity tended to stabilize at 964 mAh·g^{-1} after 16 cycles. By combining electrospinning, hydrothermal treatment, and post annealing, Reddy *et al.* fabricated a γ-Fe_2O_3-carbon nanofiber hybrid.[92] At a current density of 50 mA·g^{-1}, the γ-Fe_2O_3-CNF hybrid delivered a specific capacity of 830 mAh·g^{-1} after 40 cycles.

γ-Fe_2O_3 based 2D nanostructures

The reports on γ-Fe_2O_3 based 2D nanostructured anodes are relatively rare.[95-97] Lee *et al.* reported a γ-Fe_2O_3-C porous microdisc anode material (Figure 5c).[95] The synthesis involved two steps: hydrothermal synthesis of α-Fe_2O_3 porous discs and CVD post-treatment in acetylene atmosphere. During the CVD treatment, the α-Fe_2O_3 was converted into γ-Fe_2O_3 and a thin carbon shell was coated onto the surface of the sample. The combination of abundant porosity and thin carbon coating provided fast diffusion for both Li^+ and electrons. A high capacity of over 900 mAh·g^{-1} could be achieved after 40 cycles at 0.1 C. A γ-Fe_2O_3-RGO composite was fabricated by Yushin and co-workers (Figure 5d).[97] The γ-Fe_2O_3-RGO composite exhibited a high specific capacity of 690 mAh·g^{-1} after 100 cycles at 0.5 C.

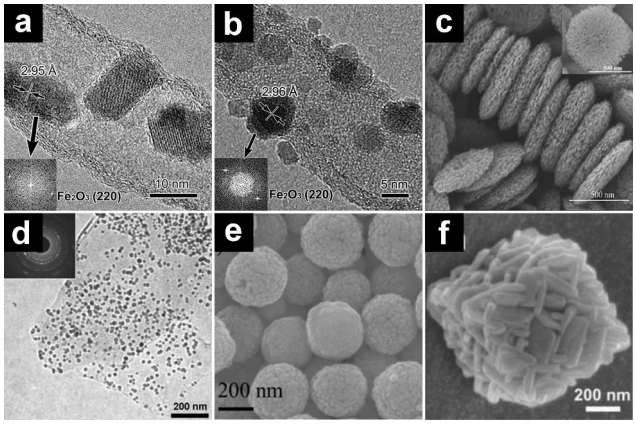

Figure 5 TEM images of γ-Fe_2O_3 nanoparticle-filled CNT (a) and γ-Fe_2O_3 nanoparticle-coated CNT (b);[91] SEM image of γ-Fe_2O_3-C porous microdiscs (c);[95] TEM image of γ-Fe_2O_3-graphene composite (d);[97] SEM image of *N*-doped carbon coated γ-Fe_2O_3 spheres (e);[100] SEM image of Fe_2O_3 hierarchical hollow microbox (f).[102]

γ-Fe_2O_3 based 3D nanostructures

A variety of γ-Fe_2O_3 based 3D architectures have been applied in lithium storage, including γ-Fe_2O_3 microspheres,[98,99] *N*-doped carbon coated γ-Fe_2O_3 spheres (Figure 5e),[100] γ-Fe_2O_3 hollow nanoparticles,[101] Fe_2O_3 hierarchical hollow microboxes (Figure 5f),[102,103] hollow γ-Fe_2O_3@graphene core@shell hybrid,[104] polypyrrole coated γ-Fe_2O_3-ordered mesoporous carbon,[105] and double-shelled Fe_2O_3-Co_3O_4 hollow microcubes.[106] For example, monodisperse γ-Fe_2O_3 mesoporous spheres were fabricated by a surfactant-free solvothermal method with subsequent thermal transformation.[99] The resultant γ-Fe_2O_3 mesoporous spheres with an average diameter of 6 μm were composed of numerous irregular shaped nanoparticles. When explored as the anode material for LIBs, the γ-Fe_2O_3 mesoporous microspheres exhibited a high initial capacity of 1453 mAh·g^{-1}, retaining ~700 mAh·g^{-1} after 110 cycles. Ding and co-workers designed a *N*-doped carbon γ-Fe_2O_3 sphere anode (Figure 5e) with high specific capacity, stable cycling, and excellent rate capability.[100] A high capacity of 870 mAh·g^{-1} could be achieved after 150 cycles at 0.5 C. Lu's group designed a delicate polypyrrole coated γ-Fe_2O_3-ordered mesoporous carbon composite.[105] Ordered mesoporous carbon was firstly synthesized via a nanocasting method, and γ-Fe_2O_3 nanoparticles were then loaded into the mesoporous carbon through wet impregnation and thermal decomposition. The polypyrrole coating was achieved by vapor-phase polymerization. When applied as the LIB anode, this novel nanocomposite delivered a capacity of 785 mAh·g^{-1} after 100 cycles at 0.2 C. The superior anode performance could be ascribed to the synergistic effect of mesoporous carbon matrix and polypyrrole sealing layer.

Magnetite based anode materials

Fe_3O_4 has an inverse spinel crystal structure. Compared to α-Fe_2O_3 and γ-Fe_2O_3, Fe_3O_4 possesses significantly enhanced electronic conductivity, which is only an order of magnitude lower than the minimum metallic conductivity.[107] Theoretically, each formular of Fe_3O_4 may react with 8 Li^+, giving rise to a high capacity of 926 mAh· g^{-1}.

Fe_3O_4-based 0D nanostructures

Important progress has been made in the synthesis and lithium storage performance of Fe_3O_4 based nanoparticles during the last decade.[108-111] For example, Guo, Song, and co-workers developed a beaker-in-autoclave setup for the synthesis of highly disperse Fe_3O_4 nanoparticles.[108] Although the obtained Fe_3O_4 nanoparticles exhibited a reversible capacity of over 600 mAh·g^{-1}, the capacity decreased to 30 mAh·g^{-1} after only 30 cycles. After carbon encapsulation, the cycling performance could be significantly enhanced; a stable capacity of above 600 mAh·g^{-1} could be achieved. In another example, Zhao *et al.* fabricated carbon nanosphere (~60 nm) encapsulated Fe_3O_4 nanocrystals (~9 nm) through a facile hydrothermal treatment-annealing process (Figure 6a).[97] The composite nanospheres manifested high specific capacities of 784, 568, and 379 mAh·g^{-1} at 1, 5, and 10 C (1 C=924 mA·g^{-1}), respectively.

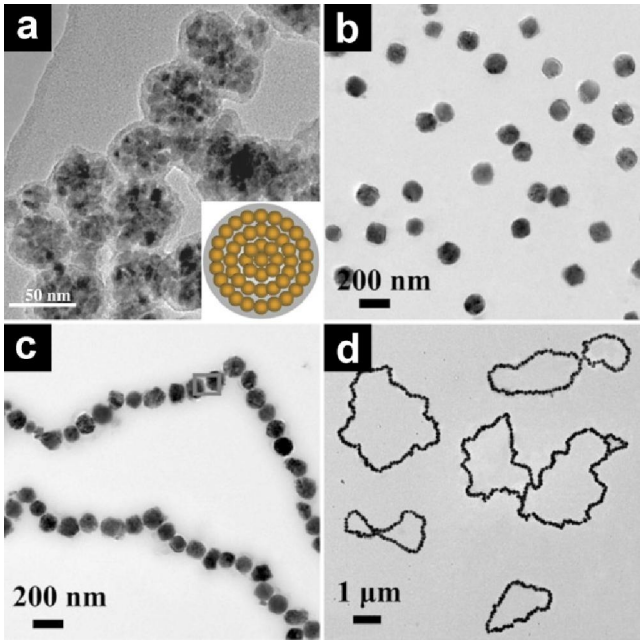

Figure 6 TEM image and schematic structure (inset) of carbon nanosphere encapsulated Fe_3O_4 nanocrystals (a);[97] TEM images of Fe_3O_4@C core-shell nanospheres (b), chains (c), and rings (d).[113]

Due to their interesting ferromagnetic properties, the 0D Fe_3O_4 based nanoparticles can be further assembled into chains and rings.[112,113] Wang, Su, and co-workers synthesized monodisperse Fe_3O_4@C core-shell spheres (Figure 6b) using eccentric Fe_2O_3@poly(acrylic acid) core-shell nanoparticles as the precursor.[113] By adjusting the reaction temperature and time, Fe_3O_4@C core-shell chains (Figure 6c) and rings (Figure 6d) could also be obtained. When tested as anode materials for LIBs, the Fe_3O_4@C core-shell chains and rings delivered capacities of 780–800 mAh·g^{-1} after 100 cycles at 200 mA·g^{-1}, much higher than that of Fe_3O_4@C core-shell nanospheres.

Fe_3O_4-based 1D nanostructures

More than a decade ago, Fe_3O_4 had been electrochemically deposited onto Cu nanorod arrays for lithium storage.[107] The self-supported Cu-nanorod Fe_3O_4 electrode demonstrated excellent rate capability. When compared to planar electrodes, the power density could be improved by a factor of six. Since then, much attention has been paid to 1D Fe_3O_4 based nanostructures for lithium storage.[114-121] Fe_3O_4 based 1D nanofibers/nanotubes can be facilely prepared via electrospinning.[122-126] Chen *et al.* prepared Fe_3O_4-C composite nanofibers via electrospinning ferric acetylacetonate and polyacrylonitrile (PAN) with subsequent annealing.[122] A high specific capacity of 1007 mAh·g^{-1} could be obtained after 80 cycles at 200 mA·g^{-1}. The electrospinning technique can be easily extended to the fabrication of Fe_3O_4-C hollow nanofibers[123,124] Fe_3O_4-TiO_2 nanofiber,[125] and *N*-doped amorphous carbon coated Fe_3O_4-SnO_2 coaxial nanofibers (Figure 7a).[126]

Carbon nanotubes (CNTs) have been extensively used as the backbone material to construct Fe_3O_4 based 1D nanostructures.[127-131] For example, Dillon *et al.* designed a binder-free Fe_3O_4 nanorod-SWCNT electrode (Figure 7b) through a two-step vacuum filtration-reduction process.[127] Impressively, the binder-free electrode with 95 wt% Fe_3O_4 and 5 wt% SWCNT demonstrated high reversible capacities of ~1000, 800, and 600 mAh·g^{-1} at 1, 5, and 10 C, respectively. By integrating CNT drawing and magnetron sputtering, Wang *et al.* obtained Fe_3O_4-CNT electrodes.[128] The Fe_3O_4 nanoparticles with sizes of 5–7 nm were uniformly sputtered on aligned CNTs, forming a core-sheath structure (Figures 7c and 7d). The free-standing Fe_3O_4-CNT electrode delivered a specific capacity of over 800 mAh·g^{-1} based on the total mass of the electrode. Benefitting from the outstanding electronic conductivity of CNTs, the electrode also demonstrated excellent rate capability.

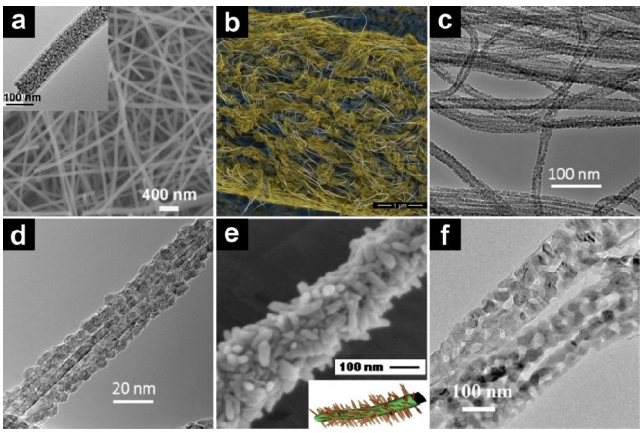

Figure 7 SEM and TEM (inset) images of *N*-doped amorphous carbon coated Fe_3O_4-SnO_2 coaxial nanofibers (a); [126] colorized SEM image of Fe_3O_4 nanorod-SWC NT composite (b); [127] TEM images of core-sheath structured Fe_3O_4-CNT composites (c, d);[128] SEM image and schematic illustration of Fe_3O_4-TiO_2-C composite nanofibers (e);[132] and TEM image of porous Fe_3O_4-VO_x-graphene ternary nanowires (f).[136]

Cellulose nanofibers and other 1D nanostructures can also be employed as the scaffold material or sacrificial templates to prepare 1D Fe_3O_4 based nanofibers/nanowires/nanotubes.[132-136] Huang *et al.* constructed Fe_3O_4-TiO_2-C composite nanofibers (Figure 7e) by employing natural cellulose as the scaffold.[132] The ternary composite exhibited a stable capacity of ~525 mAh·g^{-1} at 100 mA·g^{-1}. By anchoring Fe_2O_3 nanoparticles on bacterial cellulose nanofiber followed by carbonization, Luo and co-workers obtained a flexible, binder-free Fe_3O_4-carbon nanofiber electrode.[133] By electrochemical deposition of Fe_3O_4 on CuO nanoneedle arrays, Yan *et al.* obtained coaxial CuO@Fe_3O_4 hybrid nanowire electrode.[134] Lu's group reported the synthesis of carbon coated Fe_3O_4 nanotubes by using α-MoO_3 nanorods as the hard template.[135] An *et al.* synthesized porous Fe_3O_4-amorphous vanadium oxide-graphene (Fe_3O_4-VO_x-graphene) ternary nanowires (Figure 7f) by reducing graphene decorated iron vanadate ($FeVO_4 \cdot 1.1H_2O$) nanowires in 5%/95% H_2/Ar.[136]

Fe_3O_4-based 2D nanostructures

Fe_3O_4-graphene nanocomposite is the most extensively studied Fe_3O_4-based 2D nanostructures.[137-149] In 2010, Cheng's group designed a graphene nanosheets wrapped Fe_3O_4 (Figures 8a and 8b) anode.[137] In the constructed Fe_3O_4-graphene composite, the graphene nanosheets not only buffered the volume change of Fe_3O_4, but also acted as the electron highway; the Fe_3O_4 particles prevented the restacking of graphene; meanwhile, the porosity between Fe_3O_4 and graphene provided efficient Li^+ diffusion channels. As a result, the resultant Fe_3O_4-graphene nanocomposite delivered a specific capacity of 580 mAh·g^{-1} after 100 cycles at 700 mA·g^{-1} (Figure 8c). More recently, an intriguing Fe_3O_4 nanoparticle-TiO_2 nanorod-graphene sheet (Fe_3O_4-TiO_2-Graphene) ternary hetero-structured anode was reported by Liu, Xie, and co-workers (Figures 8d and 8e).[148] The Fe_3O_4-TiO_2-Graphene ternary composite delivered a reversible capacity of ~330 mAh·g^{-1} at 1000 mA·g^{-1} (Figure 8f).

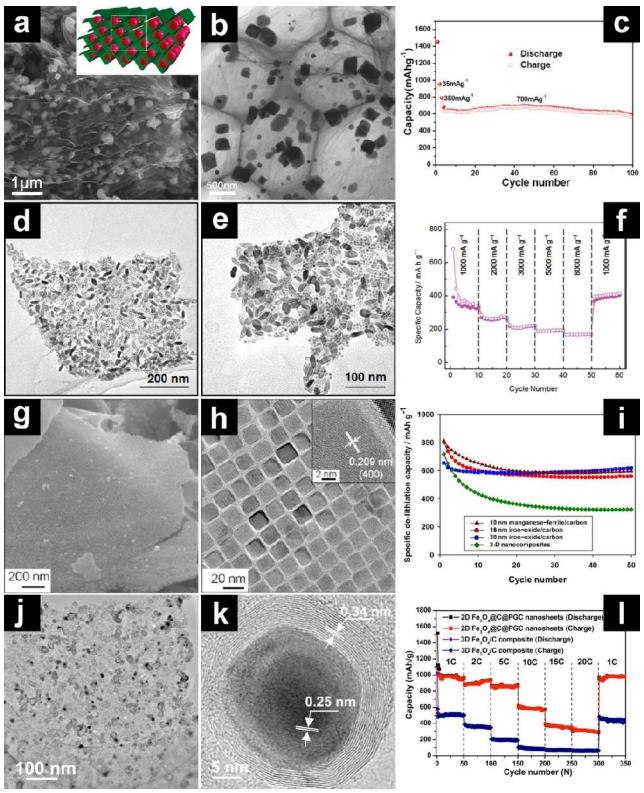

Figure 8 Schematic illustration (inset), SEM image (a), TEM image (b) and cycling performance (c) of Fe_3O_4-graphene nanocomposite;[137] TEM images (d, e) and rate performance (f) of Fe_3O_4-TiO_2-graphene ternary hetero-structures;[148] SEM image (g), TEM image (h), and cycling performance (i) of Fe_3O_4 nanocrystal-carbon hybrid nanosheets;[150] TEM image (j), high-resolution TEM (k) image, and rate performance (l) of Fe_3O_4 nanoparticle-graphitic carbon hybrid nanosheets.[151]

2D Fe_3O_4-C hybrid nanosheets have also been prepared for lithium storage.[150-152] Hyeon, Piao, and co-workers presented a simple and direct synthetic approach for the fabrication of Fe_3O_4 nanocrystal-carbon hybrid nanosheets (Figures 8g and 8h) using ferric oleate complex as the precursor for both Fe_3O_4 and carbon.[150] Sodium sulfate was used as the template for producing the 2D nanosheet structures. Interestingly, the Fe_3O_4 nanocrystals embedded in the carbon nanosheets were very uniform and their size could be well controlled by tuning the heating rate and temperature. The 2D Fe_3O_4 nanocrystal-carbon hybrid nanosheets exhibited stable capacities of ~600 mAh·g^{-1} and size dependant rate capabilities (Figure 8i). In another study, Zhao *et al.* fabricated Fe_3O_4 nanoparticle-graphitic carbon hybrid nanosheets (Figure 8j, 8k).[151] Benefiting from the outstanding structural and electrical integrity, the Fe_3O_4-graphitic carbon hybrid demonstrated excellent rate capability and cycling performance. Even at an ultrahigh current density of 20 A·g^{-1}, a capacity of 311 mAh·g^{-1} could be obtained (Figure 8l).

Fe_3O_4-based 3D nanostructures

Due to their multiple structural merits, Fe_3O_4-based hollow structures, such as hollow spheres and hollow cubes, have demonstrated promising lithium storage performances.[153-161] As a typical example, Lou *et al.* prepared uniform Fe_3O_4 hierarchical hollow spheres comprised of nanoplate building blocks (Figures 9a and 9b) by an ethylene glycol-mediated solvothermal method.[159] The product delivered a reversible capacity of 640 mAh·g^{-1} at 200 mA·g^{-1}, retaining 580 mAh·g^{-1} after 100 cycles (Figure 9c). In another study, the same group synthesized monodisperse Fe_3O_4 hollow spheres organized by ultrathin nanosheets (Figures 9d and 9e), which demonstrated a high reversible capacity of 1046 mAh·g^{-1} without noticeable capacity fading over 100 cycles.[160] Such unique structures also led to remarkable rate capability, showing capacities of 992, 853, 716, and 548 mAh·g^{-1} at 1, 2, 4, and 8 A·g^{-1}, respectively (Figure 9f).

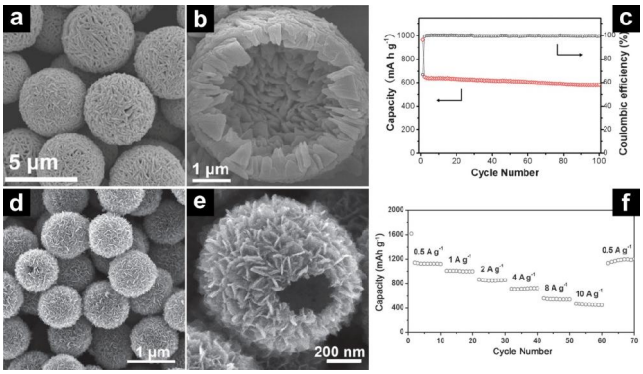

Figure 9 SEM images (a, b) and cycling performance (c) of Fe_3O_4 hierarchical hollow spheres comprised of nanoplates;[159] SEM images (d, e) and rate performance (f) of Fe_3O_4 hierarchical hollow spheres constructed by ultrathin nanosheets.[160]

With desirable free spaces for volume change accommodation, yolk@shell structures have also been fabricated to boost the electrochemical performances of Fe_3O_4.[162-166] Guan *et al.* constructed Fe_3O_4@C yolk@shell spheres (Figure 10a) showing a specific capacity of 680 mAh·g^{-1} at 5 A·g^{-1}.[162] Paik *et al.* reported the synthesis of Fe_3O_4@C yolk-shell microcubes (Figure 10b) via an "etching-in-a-box" strategy.[165] The Fe_3O_4@C yolk-shell boxes with an optimized etching time of 2 h demonstrated the best anode performance in terms of specific capacity, cycling stability, and rate capability. Guo *et al.* designed a novel yolk@shell structure with a Fe_3O_4@Fe_3C core@shell yolk and a carbon nanospindle shell (Figure 10c).[164] This intricate yolk@shell structure demonstrated significantly enhanced electrochemical performances when compared to bare Fe_3O_4 and Fe_3O_4@C core-shell structures. To study the effects of void size on the electrochemical performances, Yu, Zhou, and co-workers prepared a series of FeO_x@C yolk@shell structures (Fe_3O_4 as the dominant phase) with tailored void space (Figure 10d).[163] Only with an optimized void size, the FeO_x@C yolk@shell structures demonstrated the best cycling performance (Figure 10e).

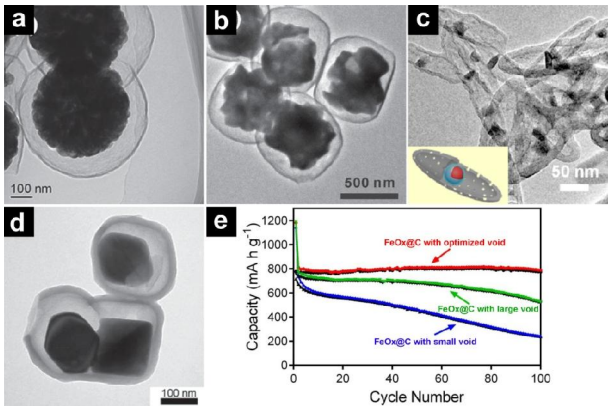

Figure 10 TEM image of Fe_3O_4@C yolk@shell spheres (a);[162] TEM image of Fe_3O_4@C yolk-shell microboxes (b);[165] TEM image of yolk@shell structures with Fe_3O_4@Fe_3C yolks and carbon nanospindle shells (c);[164] TEM image (d) and cycling performance (e) of FeO_x@C yolk-shell structures with an optimized void size.[163]

Fe_3O_4-based hierarchical structures also demonstrate high lithium storage performances. Long, Ling, and co-workers reported the preparation of Fe_3O_4-C micro-flowers constructed by nanoflakes (Figures 11a and 11b).[167] The Fe_3O_4-C microflowers delivered high specific capacities of 920–1030 mAh·g^{-1} for 150 cycles. Hyeon *et al.* reported a bottom-up self-assembly approach for the fabrication of Fe_3O_4-C hierarchical spheres comprised of nanoparticles (11–12 nm).[168] Compared to random Fe_3O_4 nanoparticle aggregates, the assembled hierarchical spheres demonstrated better cyclability and higher Coulombic efficiency.

Porous carbon materials is considered as an ideal host material to encapsulate electrochemically active Fe_3O_4 for lithium storage.[169-177] By coating α-Fe_2O_3 nanospindles with glucose-derived carbon-rich polysaccharide followed by carbothermal reduction, carbon coated Fe_3O_4 nanospindles (Fe_3O_4@C) were prepared by Wan, Guo, and co-workers (Figure 11c).[169] By chemical vapor deposition of acetylene on α-Fe_2O_3 nanorings, Zhu *et al.* obtained Fe_3O_4@C nanorings (Figure 11d); during the CVD, carbon deposition and α-Fe_2O_3 reduction occurred simultaneously.[174] Through a hydrothermal method followed by carbonization, Xue *et al.* prepared mesoporous carbon sphere encapsulated Fe_3O_4 nanoparticles (Figure 11e).[176] By impregnating $Fe(NO_3)_3$ into mesoporous carbon via a "host-guest" approach, Lee, Kim, and co-workers synthesized mesocellular carbon foam encapsulated Fe_3O_4 nanocrystals (Figure 11f).[170] All these Fe_3O_4-porous carbon nanocomposites demonstrated superior electrochemical lithium storage performances. Especially, the Fe_3O_4 nanoparticle embedded in mesoporous carbon spheres exhibited stable capacities for 290 cycles at various current densities ranging from 0.5–10 A·g^{-1}.[176]

Conclusions

This review provides a comprehensive summary on the nanostructure engineering of iron oxides (Fe_2O_3, Fe_3O_4 and γ-Fe_2O_3) for high-capacity lithium storage. Various iron oxide nanostructures, including 0D nanoparticles, 1D nanowires/nanorods/nanofibers/nanotubes, 2D nanoflakes/nanosheets, as well as 3D porous/hollow/hierarchical architectures, have been constructed for lithium storage. These delicate nanostructures show not only reduced ion/electron diffusion lengths but also sufficient free space for volume change accommodation and strain relaxation, leading to enhanced cycling stability and rate capability. Moreover, the combination of nanostructured iron oxide with conductive carbon integrates the advantages of both components, further boosting the structural stability and electrochemical performances.

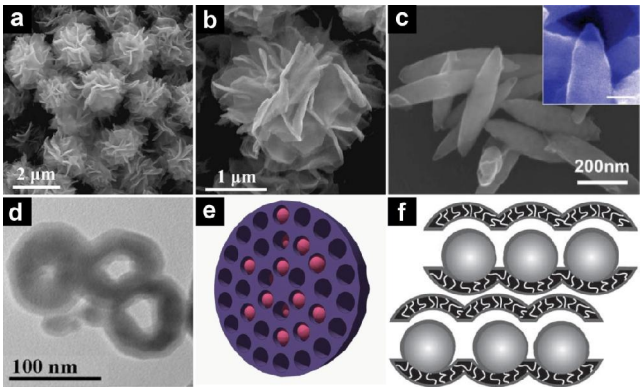

Figure 11 SEM images of Fe_3O_4-C micro-flowers (a, b); [167] SEM image of carbon coated Fe_3O_4 nanospindles (c); [169] TEM image of carbon coated Fe_3O_4 nanorings (d);[174] schematic illustration of mesoporous carbon sphere encapsulated Fe_3O_4 nanoparticles (e);[176] schematic illustration of mesocellular carbon foam encapsulated Fe_3O_4 nanocrystals (f).[170]

Despite the design of iron oxide nanostructures and the hybridization of iron oxide with conductive carbon could address the volume change issue and improve the cyclability effectively, some other issues still remain for iron oxide based anode materials. These issues include: (1) the low initial Coulombic efficiency of iron oxide base anode materials, (2) the relatively high charge plateau of iron oxide, and (3) the large voltage hysteresis between charge and discharge. Before the practical application of iron oxides in LIBs, these issues should be overcome. With the further development of nanostructure engineering, it is believed that the iron oxides would play a significant role in next-generation LIBs as high-performance anode materials.

Acknowledgement

This work was supported by the National Key Research and Development Program of China (2016YFA0202603), the National Basic Research Program of China (2013CB934103), the Programme of Introducing Talents of Discipline to Universities (B17034), the National Natural Science Foundation of China (51521001, 51602239, 21673171, 51502226), the National Natural Science Fund for Distinguished Young Scholars (51425204), the Hubei Provincial Natural Science Foundation of China (2016CFB267), and the Fundamental Research Funds for the Central Universities (WUT: 2016III001, 2016III002, 2016III003, 2016IVA090, 2017III009, 2017III008, 2017III007).

References

[1] Tarascon, J. M.; Armand, M. *Nature* **2001**, *414*, 359.
[2] Armand, M.; Tarascon, J. M. *Nature* **2008**, *451*, 652.
[3] Dunn, B.; Kamath, H.; Tarascon, J.-M. *Science* **2011**, *334*, 928.
[4] Cabana, J.; Monconduit, L.; Larcher, D.; Palacín, M. R. *Adv. Mater.* **2010**, *22*, E170.
[5] Wu, H.; Cui, Y. *Nano Today* **2012**, *7*, 414.
[6] Zhu, G.-N.; Wang, Y.-G.; Xia, Y.-Y. *Energy Environ. Sci.* **2012**, *5*, 6652.
[7] Chen, Z.; Belharouak, I.; Sun, Y. K.; Amine, K. *Adv. Funct. Mater.* **2013**, *23*, 959.
[8] Dylla, A. G.; Henkelman, G.; Stevenson, K. J. *Acc. Chem. Res.* **2013**, *46*, 1104.
[9] Reddy, M. V.; Subba Rao, G. V.; Chowdari, B. V. R. *Chem. Rev.* **2013**, *113*, 5364.
[10] Xu, W.; Wang, J.; Ding, F.; Chen, X.; Nasybulin, E.; Zhang, Y.; Zhang,

J.-G. *Energy Environ. Sci.* **2014**, *7*, 513.
[11] Zhao, Y.; Li, X.; Yan, B.; Xiong, D.; Li, D.; Lawes, S.; Sun, X. *Adv. Energy Mater.* **2016**, *6*, 1502175.
[12] Yu, S.-H.; Lee, S. H.; Lee, D. J.; Sung, Y.-E.; Hyeon, T. *Small* **2016**, *12*, 2146.
[13] Lin, D.; Liu, Y.; Cui, Y. *Nat. Nanotechnol.* **2017**, *12*, 194.
[14] Guo, Y.; Li, H.; Zhai, T. *Adv. Mater.* **2017**, *29*, 1700007.
[15] Xin, S.; You, Y.; Wang, S.; Gao, H.-C.; Yin, Y.-X.; Guo, Y.-G. *ACS Appl. Mater. Interfaces* **2017**, *2*, 1385.
[16] Zhao, Y.; Wang, L. P.; Sougrati, M. T.; Feng, Z.; Leconte, Y.; Fisher, A.; Srinivasan, M.; Xu, Z. *Adv. Energy Mater.* **2017**, *7*, 1601424.
[17] Poizot, P.; Laruelle, S.; Grugeon, S.; Dupont, L.; Tarascon, J. M. *Nature* **2000**, *407*, 496.
[18] Zhang, L.; Wu, H. B.; Lou, X. W. *Adv. Energy Mater.* **2014**, *4*, 1300958.
[19] Zhou, W.; Guo, L. *Chem. Soc. Rev.* **2015**, *44*, 6697.
[20] Lin, Y.-M.; Abel, P. R.; Heller, A.; Mullins, C. B. *J. Phys. Chem. Lett.* **2011**, *2*, 2885.
[21] Bruce, P. G.; Scrosati, B.; Tarascon, J.-M. *Angew. Chem., Int. Ed.* **2008**, *47*, 2930.
[22] Guo, Y.-G.; Hu, J.-S.; Wan, L.-J. *Adv. Mater.* **2008**, *20*, 2878.
[23] Sun, Y.; Liu, N.; Cui, Y. *Nat. Energy* **2016**, *1*, 16071.
[24] Sivula, K.; Le Formal, F.; Grätzel, M. *ChemSusChem* **2011**, *4*, 432.
[25] Mai, L.; Tian, X.; Xu, X.; Chang, L.; Xu, L. *Chem. Rev.* **2014**, *114*, 11828.
[26] Wu, C.; Yin, P.; Zhu, X.; OuYang, C.; Xie, Y. *J. Phys. Chem. B* **2006**, *110*, 17806.
[27] Zeng, S.; Tang, K.; Li, T. *J. Colloid Interfaces Sci.* **2007**, *312*, 513.
[28] Liu, H.; Wang, G.; Park, J.; Wang, J.; Liu, H.; Zhang, C. *Electrochim. Acta* **2009**, *54*, 1733.
[29] Liu, H.; Wexler, D.; Wang, G. *J. Alloys Compd.* **2009**, *487*, L24.
[30] Song, Y.; Qin, S.; Zhang, Y.; Gao, W.; Liu, J. *J. Phys. Chem. C* **2010**, *114*, 21158.
[31] Yao, X.; Tang, C.; Yuan, G.; Cui, P.; Xu, X.; Liu, Z. *Electrochem. Commun.* **2011**, *13*, 1439.
[32] Tartaj, P.; Amarilla, J. M. *J. Power Sources* **2011**, *196*, 2164.
[33] Zhao, K.; Wen, M.; Dong, Y.; Zhang, L.; Yan, M.; Xu, W.; Niu, C.; Zhou, L.; Wei, Q.; Ren, W.; Wang, X.; Mai, L. *Adv. Energy Mater.* **2017**, *7*, 1601582.
[34] Chen, J.; Xu, L.; Li, W.; Gou, X. *Adv. Mater.* **2005**, *17*, 582.
[35] Wang, Z.; Luan, D.; Madhavi, S.; Li, C. M.; Lou, X. W. *Chem. Commun.* **2011**, *47*, 8061.
[36] Liu, J.; Li, Y.; Fan, H.; Zhu, Z.; Jiang, J.; Ding, R.; Hu, Y.; Huang, X. *Chem. Mater.* **2010**, *22*, 212.
[37] Chaudhari, S.; Srinivasan, M. *J. Mater. Chem.* **2012**, *22*, 23049.
[38] Zeng, W.; Zheng, F.; Li, R.; Zhan, Y.; Li, Y.; Liu, J. *Nanoscale* **2012**, *4*, 2760.
[39] Ji, L.; Toprakci, O.; Alcoutlabi, M.; Yao, Y.; Li, Y.; Zhang, S.; Guo, B.; Lin, Z.; Zhang, X. *ACS Appl. Mater. Interfaces* **2012**, *4*, 2672.
[40] Zhang, X.; Liu, H.; Petnikota, S.; Ramakrishna, S.; Fan, H. J. *J. Mater. Chem. A* **2014**, *2*, 10835.
[41] Cho, J. S.; Hong, Y. J.; Kang, Y. C. *ACS Nano* **2015**, *9*, 4026.
[42] Yu, W.-J.; Hou, P.-X.; Zhang, L.-L.; Li, F.; Liu, C.; Cheng, H.-M. *Chem. Commun.* **2010**, *46*, 8576.
[43] Zhou, G.; Wang, D.-W.; Hou, P.-X.; Li, W.; Li, N.; Liu, C.; Li, F.; Cheng, H.-M. *J. Mater. Chem.* **2012**, *22*, 17942.
[44] Yu, W.-J.; Hou, P.-X.; Li, F.; Liu, C. *J. Mater. Chem.* **2012**, *22*, 13756.
[45] Zhao, Y.; Li, J.; Ding, Y.; Guan, L. *Chem. Commun.* **2011**, *47*, 7416.
[46] Reddy, M. V.; Yu, T.; Sow, C. H.; Shen, Z. X.; Lim, C. T.; Rao, G. V. S.; Chowdari, B. V. R. *Adv. Funct. Mater.* **2007**, *17*, 2792.
[47] Li, L.; Wu, H. B.; Yu, L.; Madhavi, S.; Lou, X. W. *Adv. Mater. Interfaces* **2014**, *1*, 1400050.
[48] Lu, J.; Peng, Q.; Wang, Z.; Nan, C.; Li, L.; Li, Y. *J. Mater. Chem. A* **2013**, *1*, 5232.
[49] Zhu, X.; Zhu, Y.; Murali, S.; Stoller, M. D.; Ruoff, R. S. *ACS Nano* **2011**, *5*, 3333.
[50] Zou, Y.; Kan, J.; Wang, Y. *J. Phys. Chem. C* **2011**, *115*, 20747.
[51] Wang, G.; Liu, T.; Luo, Y.; Zhao, Y.; Ren, Z.; Bai, J.; Wang, H. *J. Alloys Compd.* **2011**, *509*, L216.
[52] Xue, X.-Y.; Ma, C.-H.; Cui, C.-X.; Xing, L.-L. *Solid State Sci.* **2011**, *13*, 1526.
[53] Zhang, M.; Qu, B.; Lei, D.; Chen, Y.; Yu, X.; Chen, L.; Li, Q.; Wang, Y.; Wang, T. *J. Mater. Chem.* **2012**, *22*, 3868.
[54] Xiao, L.; Wu, D.; Han, S.; Huang, Y.; Li, S.; He, M.; Zhang, F.; Feng, X. *ACS App. Mater. Interfaces* **2013**, *5*, 3764.
[55] Qu, J.; Yin, Y.-X.; Wang, Y.-Q.; Yan, Y.; Guo, Y.-G.; Song, W.-G. *ACS Appl. Mater. Interfaces* **2013**, *5*, 3932.
[56] Su, Q.; Xie, D.; Zhang, J.; Du, G.; Xu, B. *ACS Nano* **2013**, *7*, 9115.
[57] Chen, S.; Bao, P.; Wang, G. *Nano Energy* **2013**, *2*, 425.
[58] Zhou, G.-W.; Wang, J.; Gao, P.; Yang, X.; He, Y.-S.; Liao, X.-Z.; Yang, J.; Ma, Z.-F. *Ind. Eng. Chem. Res.* **2013**, *52*, 1197.
[59] Li, L.; Zhou, G.; Weng, Z.; Shan, X.-Y.; Li, F.; Cheng, H.-M. *Carbon* **2014**, *67*, 500.
[60] Zhang, H.; Zhou, L.; Yu, C. *RSC Adv.* **2014**, *4*, 495.
[61] Chen, J. S.; Zhu, T.; Yang, X. H.; Yang, H. G.; Lou, X. W. *J. Am. Chem. Soc.* **2010**, *132*, 13162.
[62] Lou, X. W.; Archer, L. A.; Yang, Z. *Adv. Mater.* **2008**, *20*, 3987.
[63] Zhou, L.; Zhao, D.; Lou, X. W. *Adv. Mater.* **2012**, *24*, 745.
[64] Zhou, L.; Zhuang, Z.; Zhao, H.; Lin, M.; Zhao, D.; Mai, L. *Adv. Mater.* **2017**, *29*, 1602914.
[65] Lai, X.; Halpert, J. E.; Wang, D. *Energy Environ. Sci.* **2012**, *5*, 5604.
[66] Qi, J.; Lai, X.; Wang, J.; Tang, H.; Ren, H.; Yang, Y.; Jin, Q.; Zhang, L.; Yu, R.; Ma, G.; Su, Z.; Zhao, H.; Wang, D. *Chem. Soc. Rev.* **2015**, *44*, 6749.
[67] Zeng, S.; Tang, K.; Li, T.; Liang, Z.; Wang, D.; Wang, Y.; Zhou, W. *J. Phys. Chem. C* **2007**, *111*, 10217.
[68] Wu, Z.; Yu, K.; Zhang, S.; Xie, Y. *J. Phys. Chem. C* **2008**, *112*, 11307.
[69] Zhou, J.; Song, H.; Chen, X.; Zhi, L.; Yang, S.; Huo, J.; Yang, W. *Chem. Mater.* **2009**, *21*, 2935.
[70] Wang, B.; Chen, J. S.; Wu, H. B.; Wang, Z.; Lou, X. W. *J. Am. Chem. Soc.* **2011**, *133*, 17146.
[71] Wang, B.; Chen, J. S.; Lou, X. W. *J. Mater. Chem.* **2012**, *22*, 9466.
[72] Zhu, J.; Yin, Z.; Yang, D.; Sun, T.; Yu, H.; Hoster, H. E.; Hng, H. H.; Zhang, H.; Yan, Q. *Energy Environ. Sci.* **2013**, *6*, 987.
[73] Jeong, J.-M.; Choi, B. G.; Lee, S. C.; Lee, K. G.; Chang, S.-J.; Han, Y.-K.; Lee, Y. B.; Lee, H. U.; Kwon, S.; Lee, G.; Lee, C.-S.; Huh, Y. S. *Adv. Mater.* **2013**, *25*, 6250.
[74] Zhou, L.; Xu, H.; Zhang, H.; Yang, J.; B. Hartono, S.; Qian, K.; Zou, J.; Yu, C. *Chem. Commun.* **2013**, *49*, 8695.
[75] Padashbarmchi, Z.; Hamidian, A. H.; Zhang, H.; Zhou, L.; Khorasani, N.; Kazemzad, M.; Yu, C. *RSC Adv.* **2015**, *5*, 10304.
[76] Xu, S.; Hessel, C. M.; Ren, H.; Yu, R.; Jin, Q.; Yang, M.; Zhao, H.; Wang, D. *Energy Environ. Sci.* **2014**, *7*, 632.
[77] Son, M. Y.; Hong, Y. J.; Lee, J.-K.; Kang, Y. C. *Nanoscale* **2013**, *5*, 11592.
[78] Brezesinski, K.; Haetge, J.; Wang, J.; Mascotto, S.; Reitz, C.; Rein, A.; Tolbert, S. H.; Perlich, J.; Dunn, B.; Brezesinski, T. *Small* **2011**, *7*, 407.
[79] Xu, X.; Cao, R.; Jeong, S.; Cho, J. *Nano Lett.* **2012**, *12*, 4988.
[80] Xu, Y.; Jian, G.; Liu, Y.; Zhu, Y.; Zachariah, M. R.; Wang C. *Nano Energy* **2014**, *3*, 26.
[81] Cao, K.; Jiao, L.; Liu, H.; Liu, Y.; Wang, Y.; Guo, Z.; Yuan, H. *Adv. Energy Mater.* **2015**, *5*, 1401421.
[82] Zhang, H.; Sun, X.; Huang, X.; Zhou, L. *Nanoscale* **2015**, *7*, 3270.
[83] Gao, G.; Yu, L.; Wu, H. B.; Lou, X. W. *Small* **2014**, *10*, 1741.
[84] Wang, Z.; Luan, D.; Madhavi, S.; Hu, Y.; Lou, X. W. *Energy Environ. Sci.* **2012**, *5*, 5252.
[85] Wang, Y.; Xu, J.; Wu, H.; Xu, M.; Peng, Z.; Zheng, G. *J. Mater. Chem.* **2012**, *22*, 21923.
[86] Luo, J.; Xia, X.; Luo, Y.; Guan, C.; Liu, J.; Qi, X.; Ng, C. F.; Yu, T.; Zhang, H.; Fan, H. J. *Adv. Energy Mater.* **2013**, *3*, 737.
[87] Xia, H.; Xiong, W.; Lim, C. K.; Yao, Q.; Wang, Y.; Xie, J. *Nano Res.* **2014**, *7*, 1797.
[88] Zhou, W.; Cheng, C.; Liu, J.; Tay, Y. Y.; Jiang, J.; Jia, X.; Zhang, J.; Gong, H.; Hng, H. H.; Yu, T.; Fan, H. J. *Adv. Funct. Mater.* **2011**, *21*, 2439.
[89] Gu, X.; Chen, L.; Ju, Z.; Xu, H.; Yang, J.; Qian, Y. *Adv. Funct. Mater.*

2013, *23*, 4049.
[90] Kang, N.; Park, J. H.; Choi, J.; Jin, J.; Chun, J.; Jung, I. G.; Jeong, J.; Park, J.-G.; Lee, S. M.; Kim, H. J.; Son, S. U. *Angew. Chem., Int. Ed.* **2012**, *51*, 6626.
[91] Yu, W.-J.; Zhang, L.; Hou, P.-X.; Li, F.; Liu, C.; Cheng, H.-M. *Adv. Energy Mater.* **2016**, *6*, 1501755.
[92] Wu, Y.; Zhu, P.; Reddy, M. V.; Chowdari, B. V. R.; Ramakrishna, S. *ACS Appl. Mater. Interfaces* **2014**, *6*, 1951.
[93] Wu, P.; Xie, K.; Xu, X.; Li, J.; Tang, Y.; Zhou, Y.; Lu, T. *Mater. Res. Bull.* **2015**, *64*, 106.
[94] Sun, Y. F.; Zhang, J. J.; Huang, T.; Liu, Z. L.; Yu, A. S. *Int. J. Electrochem. Sci.* **2013**, *8*, 2918.
[95] Ma, Y.; Ji, G.; Lee, J. Y. *J. Mater. Chem.* **2011**, *21*, 13009.
[96] Vargas, O.; Caballero, Á.; Morales, J. *Electrochim. Acta* **2014**, *130*, 551.
[97] Kim, I. T.; Magasinski, A.; Jacob, K.; Yushin, G.; Tannenbaum, R. *Carbon* **2013**, *52*, 56.
[98] Tian, L.-L.; Zhang, M.-J.; Wu, C.; Wei, Y.; Zheng, J.-X.; Lin, L.-P.; Lu, J.; Amine, K.; Zhuang, Q.-C.; Pan, F. *ACS Appl. Mater. Interfaces* **2015**, *7*, 26284.
[99] Xu, J.-S.; Zhu, Y.-J. *ACS Appl. Mater. Interfaces* **2012**, *4*, 4752.
[100] Liang, J.; Xiao, C. H.; Chen, X.; Gao, R. X.; Ding, S. J. *Nanotechnology* **2016**, *27*, 215403.
[101] Koo, B.; Xiong, H.; Slater, M. D.; Prakapenka, V. B.; Balasubramanian, M.; Podsiadlo, P.; Johnson, C. S.; Rajh, T.; Shevchenko, E. V. *Nano Lett.* **2012**, *12*, 2429.
[102] Zhang, L.; Wu, H. B.; Madhavi, S.; Hng, H. H.; Lou, X. W. *J. Am. Chem. Soc.* **2012**, *134*, 17388.
[103] Zhang, L.; Wu, H.B .; Lou, X. W. *J. Am. Chem. Soc.* **2013**, *135*, 10664.
[104] Hu, J.; Zheng, J.; Tian, L.; Duan, Y.; Lin, L.; Cui, S.; Peng, H.; Liu, T.; Guo, H.; Wang, X.; Pan, F. *Chem. Commun.* **2015**, *51*, 7855.
[105] Han, F.; Li, D.; Li, W.-C.; Lei, C.; Sun, Q.; Lu, A.-H. *Adv. Funct. Mater.* **2013**, *23*, 1692.
[106] Li, Z.; Li, B.; Yin, L.; Qi, Y. *ACS Appl. Mater. Interfaces* **2014**, *6*, 8098.
[107] Taberna, L.; Mitra, S.; Poizot, P.; Simon, P.; Tarascon, J. M. *Nat. Mater.* **2006**, *5*, 567.
[108] Cui, Z.-M.; Jiang, L.-Y.; Song, W.-G.; Guo, Y.-G. *Chem. Mater.* **2009**, *21*, 1162.
[109] Chen, J. S.; Zhang, Y.; Lou, X. W. *ACS Appl. Mater. Interfaces* **2011**, *3*, 3276.
[110] Zhao, N.; Wu, S.; He, C.; Wang, Z.; Shi, C.; Liu, E.; Li, J. *Carbon* **2013**, *57*, 130.
[111] Lei, C.; Han, F.; Li, D.; Li, W.-C.; Sun, Q.; Zhang, X.-Q.; Lu, A.-H. *Nanoscale* **2013**, *5*, 1168.
[112] Li, L.; Wang, T.; Zhang, L.; Su, Z.; Wang, C.; Wang, R. *Chem. Eur. J.* **2012**, *18*, 11417.
[113] Wang, Y.; Zhang, L.; Gao, X.; Mao, L.; Hu, Y.; Lou, X. W. *Small* **2014**, *10*, 2815.
[114] Liu, H.; Wang, G.; Wang, J.; Wexler, D. *Electrochem. Commun.* **2008**, *10*, 1879.
[115] Muraliganth, T.; Murugan, A. V.; Manthiram, A. *Chem. Commun.* **2009**, *47*, 7360.
[116] Yuan, S. M.; Li, J. X.; Yang, L. T.; Su, L. W.; Liu, L.; Zhou, Z. *ACS Appl. Mater. Interfaces* **2011**, *3*, 705.
[117] Zhu, T.; Chen, J. S.; Lou, X. W. *J. Phys. Chem. C* **2011**, *115*, 9814.
[118] Xiong, Q. Q.; Lu, Y.; Wang, X. L.; Gu, C. D.; Qiao, Y. Q.; Tu, J. P. *J. Alloys Compd.* **2012**, *536*, 219.
[119] Xiao, Z.; Xia, Y.; Ren, Z.; Liu, Z.; Xu, G.; Chao, C.; Li, X.; Shen, G.; Han, G. *J. Mater. Chem.* **2012**, *22*, 20566.
[120] Lang, L.; Xu, Z. *ACS Appl. Mater. Interfaces* **2013**, *5*, 1698.
[121] Li, L.; Kovalchuk, A.; Fei, H.; Peng, Z.; Li, Y.; Kim, N. D.; Xiang, C.; Yang, Y.; Ruan, G.; Tour, J. M. *Adv. Energy Mater.* **2015**, *5*, 1500171.
[122] Wang, L.; Yu, Y.; Chen, P. C.; Zhang, D. W.; Chen, C. H. *J. Power Sources* **2008**, *183*, 717.
[123] Luo, H.; Huang, K.; Sun, B.; Zhong, J. *Electrochim. Acta* **2014**, *149*, 11.
[124] Im, M. E.; Pham-Cong, D.; Kim, J. Y.; Choi, H. S.; Kim. J. H.; Kim, J. P.; Kim, J.; Jeong, S. Y.; Cho, C. R. *J. Power Sources* **2015**, *284*, 392.
[125] Wang, H.; Wang, G.; Yuan, S.; Ma, D.; Li, Y.; Zhang, Y. *Nano Res.* **2015**, *8*, 1659.
[126] Xie, W.; Li, S.; Wang, S.; Xue, S.; Liu, Z.; Jiang, X.; He, D. *ACS Appl. Mater. Interfaces* **2014**, *6*, 20334.
[127] Ban, C.; Wu, Z.; Gillaspie, D. T.; Chen, L.; Yan, Y.; Blackburn, J. L.; Dillon, A. C. *Adv. Mater.* **2010**, *22*, E145.
[128] Wu, Y.; Wei, Y.; Wang, J.; Jiang, K.; Fan, S. *Nano Lett.* **2013**, *13*, 818.
[129] Ren, S.; Prakash, R.; Wang, D.; Chakravadhanula, V. S. K.; Fichtner, M. *ChemSusChem* **2012**, *5*,1397.
[130] Cheng, J.; Wang, B.; Park, C.-M.; Wu, Y.; Huang, H.; Nie, F. *Chem. Eur. J.* **2013**, *19*, 9866.
[131] Yang, L.; Hu, J.; Dong, A.; Yang, D. *Electrochim. Acta* **2014**, *144*, 235.
[132] Li, S.; Wang, M.; Luo, Y.; Huang, J. *ACS Appl. Mater. Interfaces* **2016**, *8*, 17343.
[133] Wan, Y.; Yang Z.; Xiong G.; Guo R.; Liu Z.; Luo H. *J. Power Sources* **2015**, *294*, 414.
[134] Saadat, S.; Zhu, J.; Sim, D. H.; Hng, H. H.; Yazami, R.; Yan, Q. *J. Mater. Chem. A* **2013**, *1*, 8672.
[135] Han, F.; Ma, L.; Sun, Q.; Lei, C.; Lu, A. *Nano Res.* **2014**, *7*, 1706.
[136] An, Q.; Lv, F.; Liu, Q.; Han, C.; Zhao, K.; Sheng, J.; Wei, Q.; Yan, M.; Mai, L. *Nano Lett.* **2014**, *14*, 6250.
[137] Zhou, G.; Wang, D.-W.; Li, F.; Zhang, L.; Li, N.; Wu, Z.-S.; Wen, L.; Lu, G. Q.; Cheng, H.-M. *Chem. Mater.* **2010**, *22*, 5306.
[138] Lian, P.; Zhu, X.; Xiang, H.; Li, Z.; Yang, W.; Wang, H. *Electrochim. Acta* **2010**, *56*, 834.
[139] Su, J.; Cao, M.; Ren, L.; Hu, C. *J. Phys. Chem. C* **2011**, *115*, 14469.
[140] Li, X.; Huang, X.; Liu, D.; Wang, X.; Song, S.; Zhou, L.; Zhang, H. *J. Phys. Chem. C* **2011**, *115*, 21567.
[141] Ji, L.; Tan, Z.; Kuykendall, T. R.; Aloni, S.; Xun, S.; Lin, E.; Battaglia, V.; Zhang, Y. *Phys. Chem. Chem. Phys.* **2011**, *13*, 7170.
[142] Zhou, J.; Song, H.; Ma, L.; Chen, X. *RSC Adv.* **2011**, *1*, 782.
[143] Wang, J.-Z.; Zhong, C.; Wexler, D.; Idris, N. H.; Wang, Z.-X.; Chen, L.-Q.; Liu, H.-K. *Chem. Eur. J.* **2011**, *17*, 661.
[144] Wei, W.; Yang, S.; Zhou, H.; Lieberwirth, I.; Feng, X.; Müllen, K. *Adv. Mater.* **2013**, *25*, 2909.
[145] Luo, J.; Liu, J.; Zeng, Z.; Ng, C. F.; Ma, L.; Zhang, H.; Lin, J.; Shen, Z.; Fan, H. J. *Nano Lett.* **2013**, *13*, 6136.
[146] Wang, R.; Xu, C.; Sun, J.; Gao, L.; Lin, C. *J. Mater. Chem. A* **2013**, *1*, 1794.
[147] Zhao, L.; Gao, M.; Yue, W.; Jiang, Y.; Wang, Y.; Ren, Y.; Hu, F. *ACS Appl. Mater. Interfaces* **2015**, *7*, 9709.
[148] Pan, L.; Zhu, X.-D.; Xie, X.-M.; Liu, Y.-T. *Adv. Funct. Mater.* **2015**, *25*, 3341.
[149] Fan, L.; Li, B.; Rooney, D. W.; Zhang, N.; Sun, K. *Chem. Commun.* **2015**, *51*, 1597.
[150] Jang, B.; Park, M.; Chae, O. B.; Park, S.; Kim, Y.; Oh, S. M.; Piao, Y.; Hyeon, T. *J. Am. Chem. Soc.* **2012**, *134*, 15010.
[151] He, C.; Wu, S.; Zhao, N.; Shi, C.; Liu, E.; Li, J. *ACS Nano* **2013**, *7*, 4459.
[152] Wu, S.; Wang, Z.; He, C.; Zhao, N.; Shi, C.; Liu, E.; Li, J. *J. Mater. Chem. A* **2013**, *1*, 11011.
[153] Chen, D.; Ji, G.; Ma, Y.; Lee, J. Y.; Lu, J. *ACS Appl. Mater. Interfaces* **2011**, *3*, 3078.
[154] Lim, H.-S.; Jung, B.-Y.; Sun, Y.-K.; Suh, K.-D. *Electrochim. Acta* **2012**, *75*, 123.
[155] Zhang, J.; Yao, Y.; Huang, T.; Yu, A. *Electrochim. Acta* **2012**, *78*, 502.
[156] Chen, Y.; Xia, H.; Lu, L.; Xue, J. *J. Mater. Chem.* **2012**, *22*, 5006.
[157] Xiong, Q. Q.; Tu, J. P.; Lu, Y.; Chen, J.; Yu, Y. X.; Qiao, Y. Q.; Wang, X. L.; Gu, C. D. *J. Phys. Chem. C* **2012**, *116*, 6495.
[158] Zhang, Q.; Shi, Z.; Deng, Y.; Zheng, J.; Liu, G.; Chen, G. *J. Power Sources* **2012**, *197*, 305.
[159] Wang, B.; Wu, H. B.; Zhang, L.; Lou, X. W. *Angew. Chem., Int. Ed.* **2013**, *52*, 4165.
[160] Ma, F.-X.; Hu, H.; Wu, H. B.; Xu, C.-Y.; Xu, Z.; Zhen, L.; Lou, X. W. *Adv. Mater.* **2015**, *27*, 4097.
[161] Liu, J.; Xu, X.; Hu, R.; Yang, L.; Zhu, M. *Adv. Energy Mater.* **2016**, *6,* 1600256.

[162] Zhao, Y.; Li, J.; Wu, C.; Ding, Y.; Guan, L. *ChemPlusChem* **2012**, *77*, 748.
[163] Zhang, H.; Zhou, L.; Noonan, O.; Martin, D. J.; Whittaker, A. K.; Yu, C. *Adv. Funct. Mater.* **2014**, *24*, 4337.
[164] Zhang, J.; Wang, K.; Xu, Q.; Zhou, Y.; Cheng, F.; Guo, S. *ACS Nano* **2015**, *9*, 3369.
[165] Liu, Z.; Yu, X.-Y.; Paik, U. *Adv. Energy Mater.* **2016**, *6*, 1502318.
[166] Yang, L.; Guo, G.; Sun, H.; Shen, X.; Hu, J.; Dong, A.; Yang, D. *Electrochim. Acta* **2016**, *190*, 797.
[167] Jin, S.; Deng, H.; Long, D.; Liu, X.; Zhan, L.; Liang, X.; Qiao, W.; Ling, L. *J. Power Sources* **2011**, *196*, 3887.
[168] Lee, S. H.; Yu, S.-H.; Lee, J. E.; Jin, A.; Lee, D. J.; Lee, N.; Jo, H.; Shin, K.; Ahn, T.-Y.; Kim, Y.-W.; Choe, H.; Sung, Y.-E.; Hyeon, T. *Nano Lett.* **2013**, *13*, 4249.
[169] Zhang, W.-M.; Wu, X.-L.; Hu, J.-S.; Guo, Y.-G.; Wan, L.-J. *Adv. Funct. Mater.* **2008**, *18*, 3941.
[170] Kang, E.; Jung, Y. S.; Cavanagh, A. S.; Kim, G.-H.; George, S. M.; Dillon, A. C.; Kim, J. K.; Lee, J. *Adv. Funct. Mater.* **2011**, *21*, 2430.
[171] Yoon, T.; Chae, C.; Sun, Y.-K.; Zhao, X.; Kung, H. H.; Lee, J. K. *J. Mater. Chem.* **2011**, *21*, 17325.
[172] Latorre-Sanchez, M.; Primo, A.; Garcia, H. *J. Mater. Chem.* **2012**, *22*, 21373.
[173] Banerjee, A.; Gokhale, R.; Bhatnagar, S.; Jog, J.; Bhardwaj, M.; Lefez, B.; Hannoyer, B.; Ogale, S. *J.Mater. Chem.* **2012**, *22*, 19694.
[174] Wang, L.; Liang, J.; Zhu, Y.; Mei, T.; Zhang, X.; Yang, Q.; Qian, Y. *Nanoscale* **2013**, *5*, 3627.
[175] Su, L.; Zhong, Y.; Zhou, Z. *J. Mater. Chem. A* **2013**, *1*, 15158.
[176] Chen, Y.; Song, B.; Li, M.; Lu, L.; Xue, J. *Adv. Funct. Mater.* **2014**, *24*, 319.
[177] Wang, L.; Zhuo, L.; Zhang, C.; Zhao, F. *Chem. Eur. J.* **2014**, *20*, 4308.